Progress In Electromagnetics Research C, Vol. 138, 219–231, 2023

Metasurface Based Circularly Polarized Antenna for WI-FI Applications

Swapna Kumari Budarapu*, Metuku Shyam Sunder, and Dasari Ramakrishna

Abstract—In this paper, reactive impedance surface metasurface (RIS-MS) and negative refractive index metasurface (NRI-MS) are used to design a wideband, high gain, circularly polarized slot loaded patch antenna (SLPA) for 5 GHz WI-FI applications. The RIS-MS is utilized to improve the antenna's bandwidth. It is composed of 6×6 metallic circular patches that are periodic. To improve bandwidth, the RIS-MS is placed between the SLPA and ground plane of a conventional antenna. A metasurface lens composed of 6×6 periodic NRI metamaterial unit cells enhances the gain of the antenna. The NRI-MS superstrate is positioned at the optimal height above the conventional antenna. A prototype of the proposed antenna has been fabricated and measured experimentally. The prototype has an impedance bandwidth (IBW) of 21.7% (5.12–6.37 GHz), a 3-dB axial ratio bandwidth (ARBW) of 18.2% (5.19–6.23 GHz), and a gain of 13.5 dBic.

1. INTRODUCTION

Several wireless communication technologies, including 5 GHz Wi-fi, have been created in response to the rising demand for high-speed internet and wireless access. The 5 GHz Wi-fi frequency range has several advantages over the conventional 2.4 GHz frequency range, including quicker data transmission speeds and less interference. To effectively utilize the frequency range, however, long-range communications in the 5.150–5.850 GHz frequency band require a broadband antenna. Circularly polarised antennas (CPAs) are also required in wireless communication systems due to their resistance to polarisation mismatch, immunity to weather interference, and Faraday rotation over a wide frequency range and a great distance. Microstrip patch antennas (MPAs) are utilized extensively in wireless communication systems due to their small size, light weight, and low cost. However, their low gain, narrow bandwidth, and low efficiency prevent them from being utilized in a variety of systems.

In recent years, the use of electromagnetic metasurfaces has been widely employed to achieve a reduction in size, an enhancement in gain, and an improvement in bandwidth for MPA. Metasurfaces refer to planar structures that consist of metamaterials, often exhibiting two-dimensional characteristics [1]. Metasurfaces control the amplitude and phase of electromagnetic radiation. The structure is composed of several subwavelength components. The arrangement of these components on a flat surface can be either periodic or non-periodic. The properties of a metasurface can be manipulated and optimized by modifications to the dimensions, geometry, and configuration of its constituent elements. Numerous distinct types of metasurfaces exist, including reactive impedance surface (RIS) [2], high-impedance surface (HIS) [3], photonic band-gap surface (PBG) [4], and artificial ground structure (AGS) [5]. RIS, which consists of metallic patches arranged at regular intervals on a dielectric with a ground plane, is one of the technologies that has significantly enhanced the efficiency of CPAs [6]. RIS-MS is used for the purpose of reducing the size of antennas and enhancing their gain and bandwidth. A dipole antenna with a 45° azimuth positioned on an artificial ground plane composed of

Received 10 September 2023, Accepted 25 October 2023, Scheduled 10 November 2023
* Corresponding author: Swapna Kumari Budarapu (swapnakumaribudarapu@gmail.com).
The authors are with the University College of Engineering, Osmania University, Hyderabad, Telangana, India.

rectangular patches is proposed in [7]. This arrangement generates a 3 dB ARBW of 5.6% and an IBW of 24.6%. In [8], a RIS-based, slotted-slit MPA with asymmetric slots is proposed. The 3-dB ARBW and IBW of the proposed antenna are observed to be 2.1% and 9.5%, respectively. A compact patch antenna with a RIS substrate is designed in [9]. The 3 dB ARBW is 2.58% while the IBW is 11.16%.

Metasurface based superstrate antennas have emerged as a promising method for enhancing gain in antenna systems. Changing the radiating characteristics of a conventional antenna with a metasurface layer can result in the increase in gain. The proposed design in [10] introduces a slotted antenna with a fractal shape, accompanied by a metasurface composed of a double negative (DNG) metamaterial. This configuration exhibits desirable characteristics such as compact size, high gain, and directional properties. The antenna has a gain of 7.4 dBic and IBW of 7.6%, in the operating frequency range. In order to enhance gain, [11] proposes an MPA with a zero index metamaterial (ZIM) superstrate. IBW of the prototype is 6.57 percent. Having a maximum gain of 12.31 dBic, the 3-dB ARBW is 6.87 percent. In [12], a design for a wideband, high-gain slot antenna using a Fabry-Perot cavity equipped with a partially reflecting surface (PRS) is presented. The antenna has a 15.5% IBW, an 8.2 dB improvement in gain, and an 18.7% 3-dB ARBW. In [13], the authors designed a Fabry-Perot cavity patch antenna with a single negative metamaterial superstrate that has a broad frequency range and high gain. The proposed antenna has a maximum gain of 11.73 dB, a 3 dB ARBW of 6.29%, and an IBW of 17.32%.

This research paper presents a novel method for increasing the gain and bandwidth of a conventional patch antenna by integrating a RIS-MS and NRI-MS. The antenna under consideration has been characterized using the High-Frequency Structure Simulator (HFSS), while the measurements have been conducted inside an anechoic chamber.

2. GEOMETRY OF ANTENNA

2.1. Design of Conventional Slot-Loaded Square Patch

The single-feed slot-loaded square patch antenna (SLPA) is designed to generate right-handed circularly polarized waves and depicted in Figure 1. To generate circularly polarized radiation, two orthogonal modes with identical amplitudes and quadrature phases are required. There exist two feeding approaches that may be used for this purpose: single feed and dual feeds. However, it is worth noting that an SLPA just requires a single feed. The SLPA is designed on an FR4 ($\epsilon_r = 4.4$) substrate, and the bottom layer of the substrate works as the ground plane. On the top layer, an SLPA with dimensions $L_p \times L_p$ is positioned at a height of $H_1 = 0.8$ mm. $S_l \times S_w$ are the slot's dimensions. The polarization type of the radiated beam is determined by the direction of the slot with respect to the position of the feed (RHCP

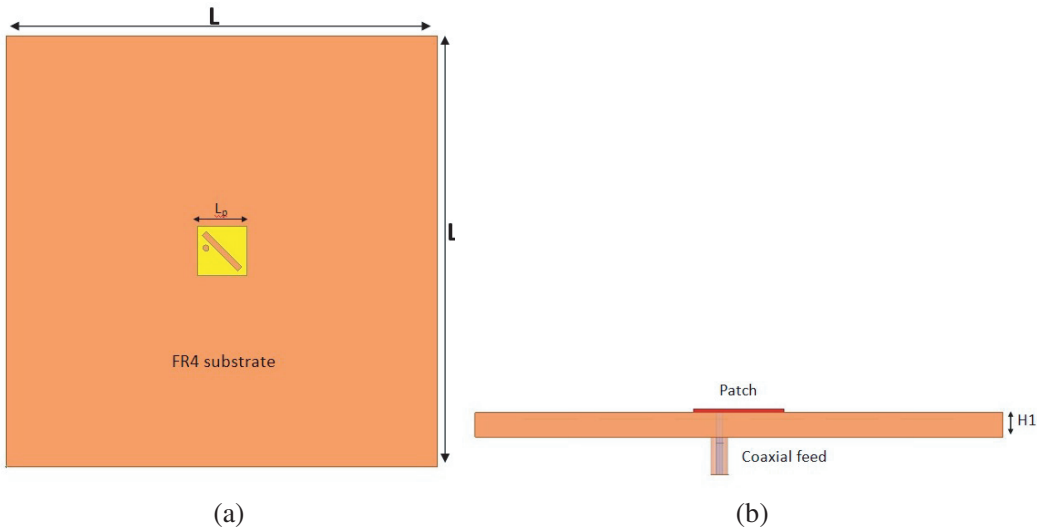

Figure 1. Conventional slot loaded patch antenna. (a) Top view. (b) Side view.

or LHCP). For probe feeding, the SMA (Sub-Miniature version A) is used. The exterior conductor of the 50 Ω SMA connector is attached to the ground plane, and the interior conductor is connected to the feed point of the patch antenna. The antenna's ground plane has dimensions of $L_g \times L_g$. The antenna has an IBW of 8.23% (5.36–5.82 GHz), a gain of 3.3 dBic, and a 3-dB ARBW of 1.6% (5.44–5.52 GHz).

2.2. The RIS-MS Loaded Antenna's Design

Figure 2 illustrates the configuration of the patch antenna with circular polarization, including the reactive impedance surface (RIS-MS). The SLPA is positioned on a substrate made of double-layer FR4 material with relative permittivity (ϵ_r) equal to 4.4. The substrate has two different thicknesses, denoted as H1 and H2. As seen in Figure 2, the ground plane is situated at the bottom layer of the substrate. A 6×6 circular RIS-MS structure is positioned between the two layers of FR4 substrates. This structure is placed at a height of H1 above the ground plane. The RIS layer comprises circular patches with dimensions of radius (c_r) and a periodicity of p, arranged in a 6×6 configuration.

The placement of RIS-MS underneath the patch antenna leads to notable enhancements in its

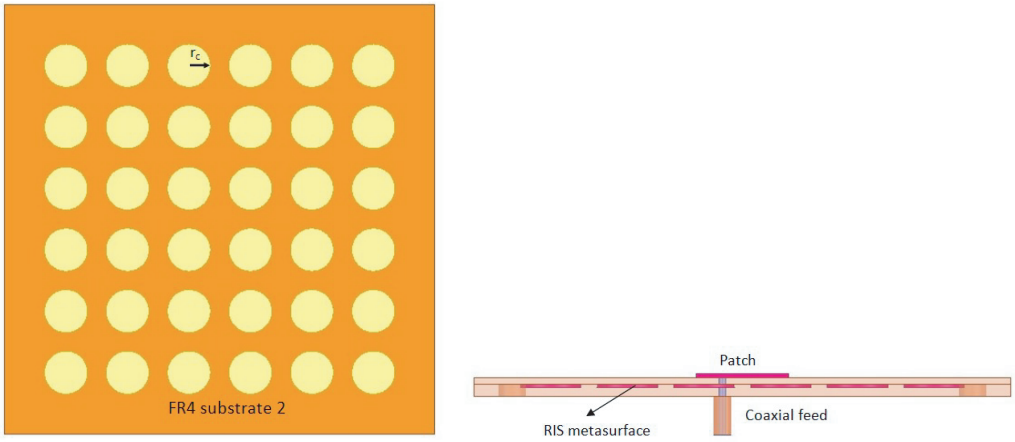

Figure 2. Conventional slot loaded patch antenna (SLPA) with reactive impedance surface based metasurface (RIS-MS). (a) Top view. (b) Side view.

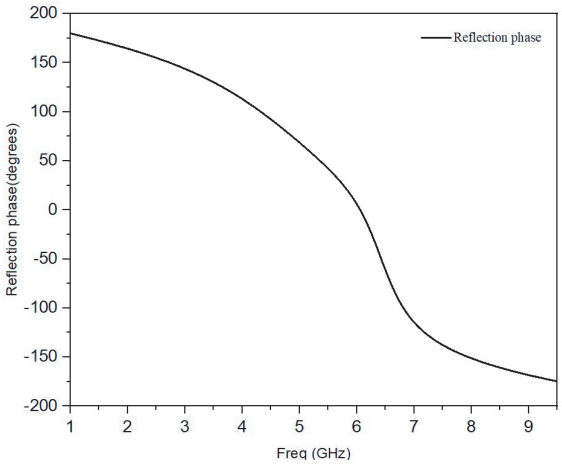

Figure 3. Reactive impedance surface based metasurface (RIS-MS) unit cell reflection phase characteristics.

IBW, ARBW, and reduction in size. The cancellation of capacitance stored underneath the SLPA by the inductive reactance of the surface leads to an increase in antenna bandwidth and a reduction in antenna size. In order to obtain an improvement of bandwidth, it is necessary to adjust the reflection phase of the RIS-MS unit cell, which is shown in Figure 3. The periodicity p of the unit cell remains constant, while the optimization of the structure is achieved by the adjustment of the parameter c_r. The operating frequency is consistently kept within the inductive zone of the RIS, which is below 6.5 GHz in this particular scenario. This is significant because an inductive phase of a RIS provides wide IBW and antenna size reduction. Hence, the antenna's dimensions have been optimized to the unit cell size (c_r) of 3.5 mm, the periodicity (p_1) of 12 mm, the height of substrate1 (H_1) of 1.6 mm, and the height of substrate2 (H_2) of 0.8 mm. The propagation of surface waves on the RIS-MS results in the generation of additional resonance and minimum points in the AR. Figure 9 demonstrates a significant improvement in the IBW and ARBW when a conventional patch is integrated with a RIS-MS. The antenna loaded with RIS-MS has an IBW of 14.66% (5.24–6.08 GHz), 3-dB ARBW of 2.72% (5.44–5.59 GHz), and gain of 4 dBic. No significant improvement in gain is observed.

2.3. Parametric Analysis

To find the optimal design parameters, a structural parametric analysis is performed on the antenna with the RIS-MS. It is important to know that when one parameter is optimized, the others remain constant. First, the impacts of the radius of RIS unit cell c_r on the antenna's CP performance are investigated. The performance of antenna is shown to be extremely sensitive to radius. The impedance bandwidth is improved, especially at lower frequencies, as seen in Figure 4(a). However, when c_r increases from 2.5 to 5.5 mm, the resultant ARBW is wider. At $c_r = 3.5$ mm, the lowest AR value exceeds 3 dB, and ARBW deteriorates. As a result, $c_r = 3.5$ mm is selected as the optimal design parameter value. Figures 4(b) and (c) depict changes in axial ratio and gain in response to variations in the c_r parameter.

To identify the optimal cell design, the AR performance for different numbers of unit cell configurations is computed. As shown in Figure 5(b), the lowest AR point for a 6×6 cell design is at 5.38 GHz, resulting in a wide axial ratio bandwidth. This is not true for cell combinations of 3×3, 4×4, and 5×5. Hence, the 6×6 cell configuration is considered. Figure 5(a) shows the variation of IBW (S_{11}) for different cell configurations.

3. THE PROPOSED ANTENNA'S DESIGN

3.1. Design of Negative Refractive Index (NRI) Metamaterial Unit Cell

The unit cell of proposed NRI-MS cell is constructed with a split ring resonator (SRR) on top of a substrate and a wire strip etched on the back of substrate. The the specifications of unit cell are as follows: The outer split ring radius (R_1) is 4.5 mm; the split gap (g) is 0.5 mm; the split ring width (w) is 1.5 mm; the space between the inner and outer rings (s) is 0.5 mm; the wire width (W_w) is 0.5 mm; and the length l_w is 9.2 mm. Figure 6 depicts the geometry of an NRI metamaterial unit cell. The fundamental electromagnetic properties of the NRI metamaterial unit cell, such as effective permeability and permittivity, have been examined. The metamaterial unit cell parameters are calculated using S-parameter retrieval method with the help of MATLAB code [14].

$$z = \pm\sqrt{\frac{(1+S_{11})^2 - S_{21}^2}{(1-S_{11})^2 - S_{21}^2}} \tag{1}$$

$$e^{jnk_0d} = \frac{S_{21}}{1 - S_{11}(\frac{z-1}{z+1})} \tag{2}$$

$$n = \frac{1}{k_0 d}[([\ln(e^{jnk_0d})]'' + 2m\pi) - j[\ln(e^{jnk_0d})]'] \tag{3}$$

where S_{11} and S_{21} are reflection and transmission coefficients; n is the refractive index; z is the impedance; k_0 is the wave number; d is the maximum length of the unit element. The permittivity and

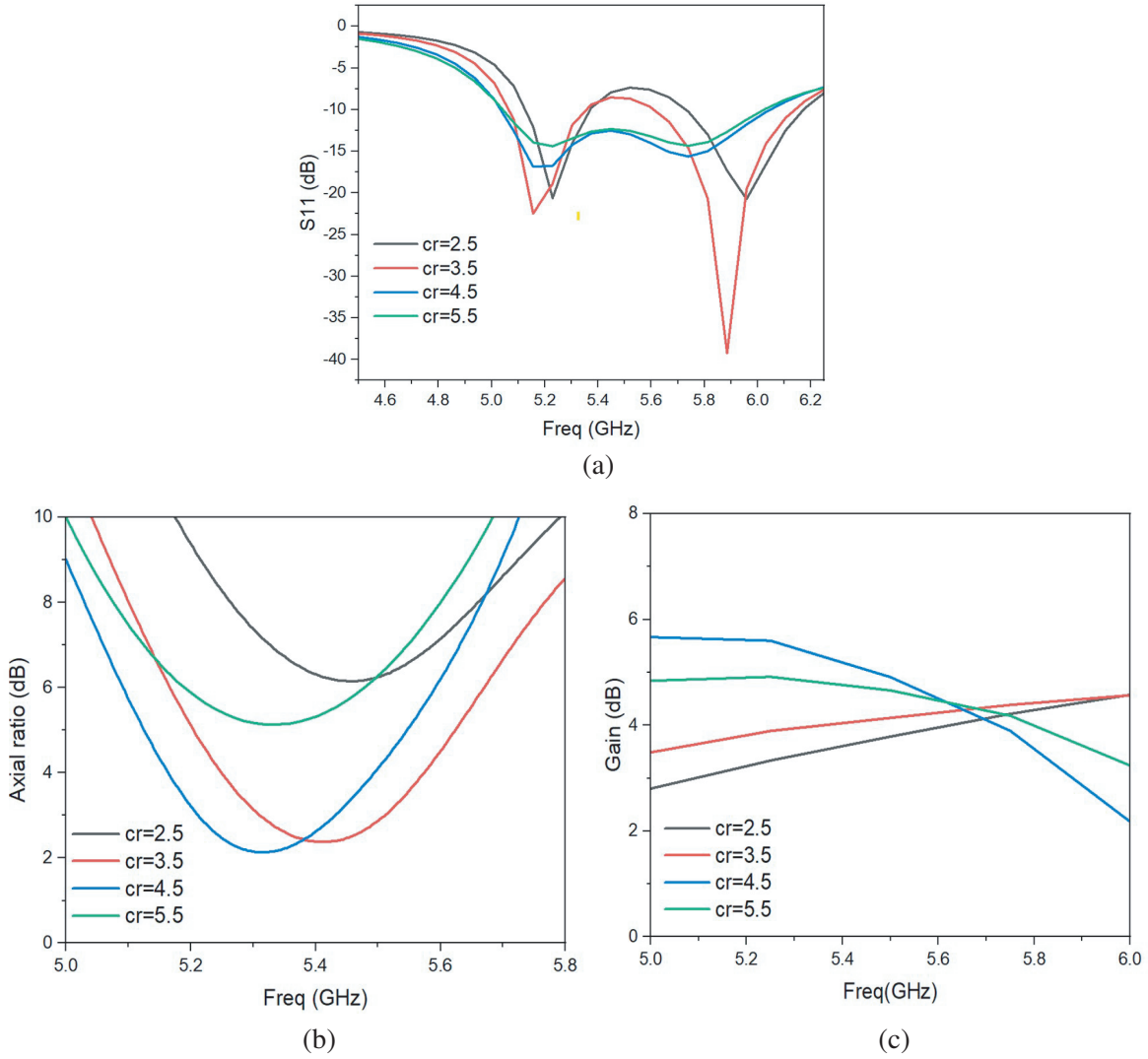

Figure 4. Simulated results of (a) reflection coefficient (S_{11}), (b) axial ratio (AR), (c) gain for different values of c_r.

permeability are related to the refractive index and impedance by the following equations

$$\epsilon = \frac{n}{z} \tag{4}$$

$$\mu = nz \tag{5}$$

Figure 7(a) illustrates real and imagined parts of the effective permeability, whereas Figure 7(b) depicts the same for effective permittivity. The unit cell effectively functions as an NRI metamaterial within the frequency range that varies from 4.5 GHz to 6.4 GHz, as demonstrated in Figure 7(c). Due to the ability of NRI materials to produce narrow beam radiation in the far field, designed structures can be used to create compact, high-gain, broad-band, reconfigurable antennas.

The NRI-MS is constructed by periodically organizing 6×6 unit cells. The periodicity of split-ring resonators is $p_2 = 10$ mm. The use of this periodic array of NRI unit cells as a superstrate has the potential to increase the performance characteristics of conventional antenna (SLPA).

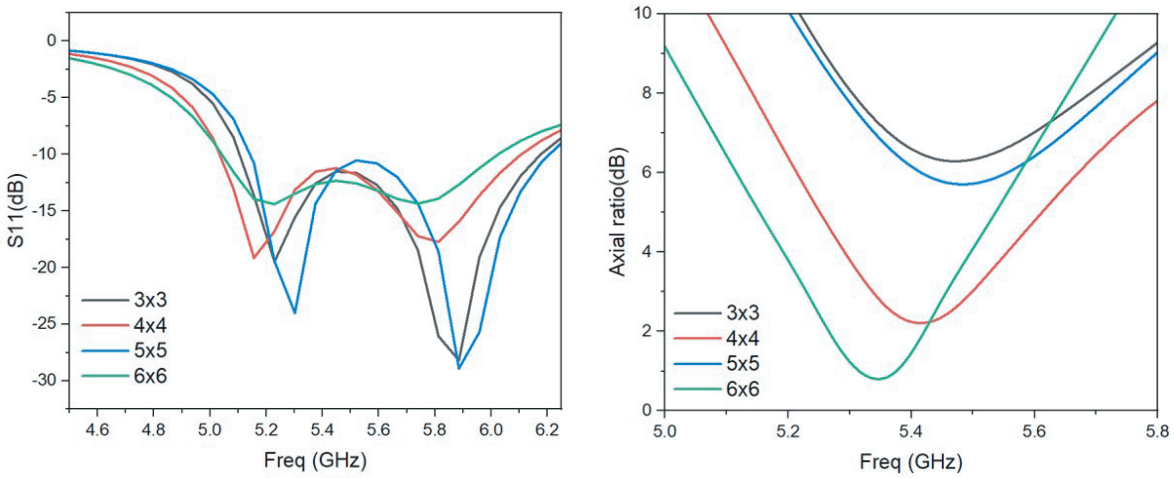

Figure 5. (a) S_{11}. (b) AR values for different cell configurations of reactive impedance surface metasurface (RIS-MS).

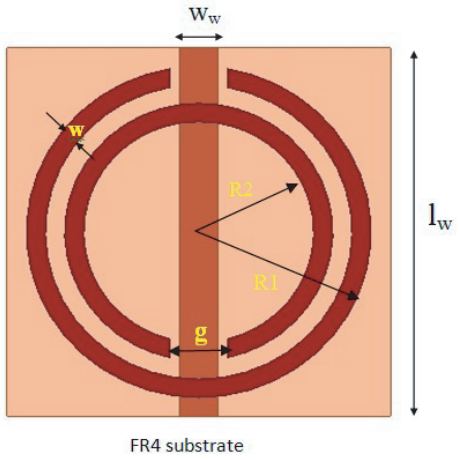

Figure 6. Geometry of NRI metamaterial unit cell.

3.2. Antenna Design Using RIS-MS and NRI-MS (Proposed Antenna)

Figures 8(a) and (b) depict the proposed RIS and NRI-MS based high-gain and wideband CP antenna's schematic diagram and geometric specifications, respectively. The antenna is composed of a probe-fed SLPA, RIS-MS, and NRI-MS. The array of NRI unit cells provides an effective refractive index that is negative in the resonant frequency of the patch antenna. When the NRI-MS is placed in the proximity to a microwave source (Antenna), it exhibits characteristics similar to those of a planar surface lens, causing the radiation pattern to be redirected towards broadside direction. This causes a reduction in the half power beam width (HPBW) and an improvement in gain.

The NRI-MS is placed over the MPA (microwave source) to function as a lens, at a height to assure optimal matching between the source and the metasurface. In the proposed design, the optimal height is 30.2 millimeters, which is roughly half the resonant wavelength. The proposed antenna is modeled in HFSS, and Figure 9 depicts the simulation results of all three antennas. The proposed antenna has a gain of 12.14 dBic. The gain of the conventional SLSP antenna is enhanced by 9 dB with the incorporation of an NRI-MS, positioned above the antenna. The impedance bandwidth (IBW) covers a frequency range of 21.8% from 5.01 to 6.23 GHz, whereas the 3-dB ARBW covers a range of 17.09%

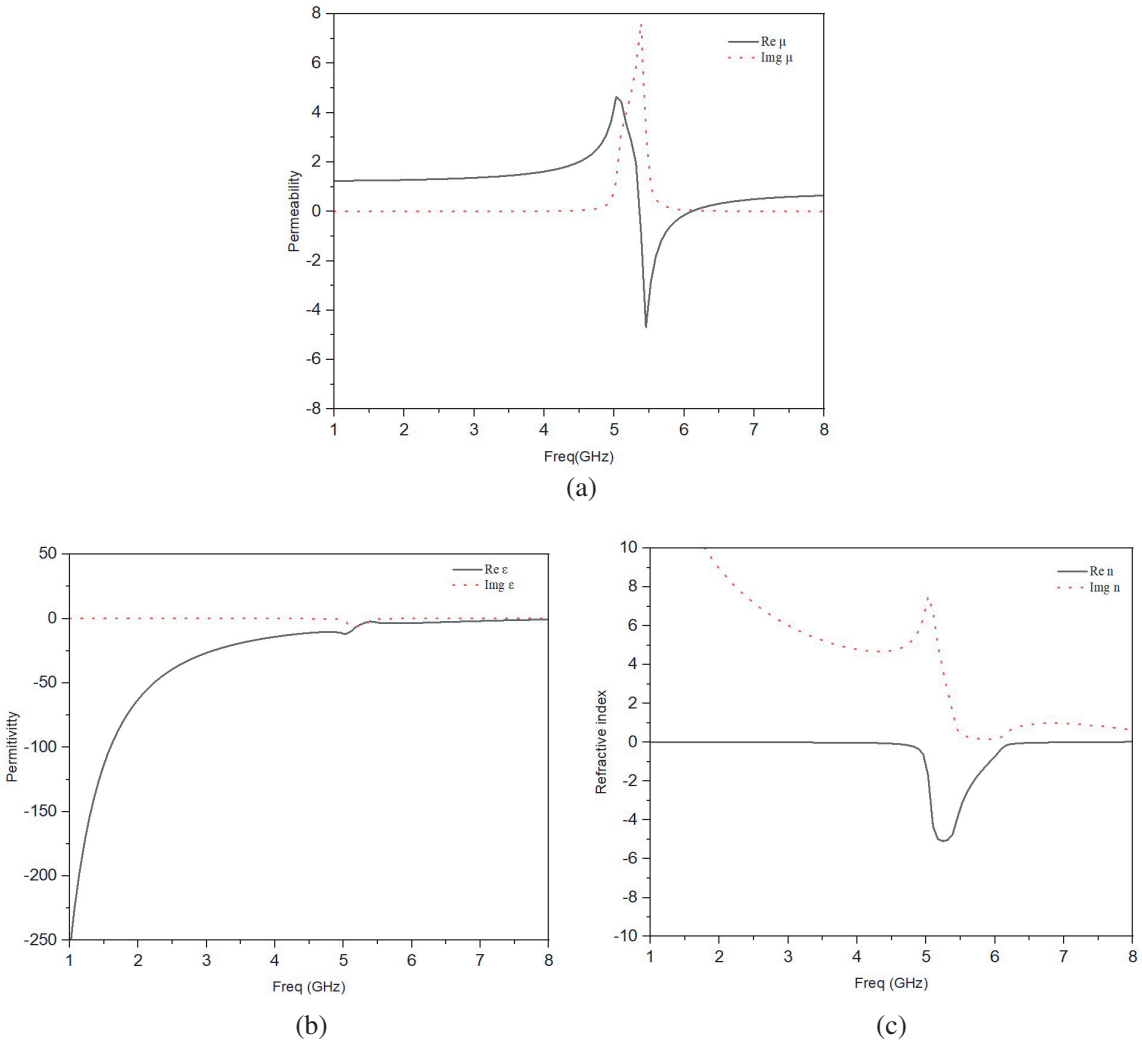

Figure 7. Parameters of NRI metamaterial unit cell. (a) Permeability (μ). (b) Permitivitty (ϵ). (c) Refractive index (n).

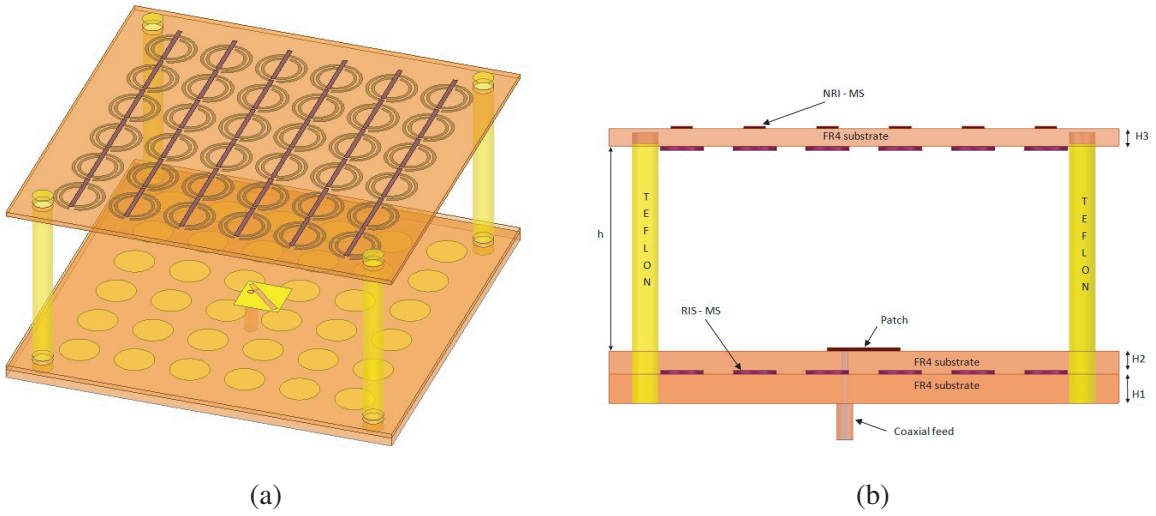

Figure 8. Proposed metasurface loaded antenna configuration. (a) 3D view. (b) Geometry (side view).

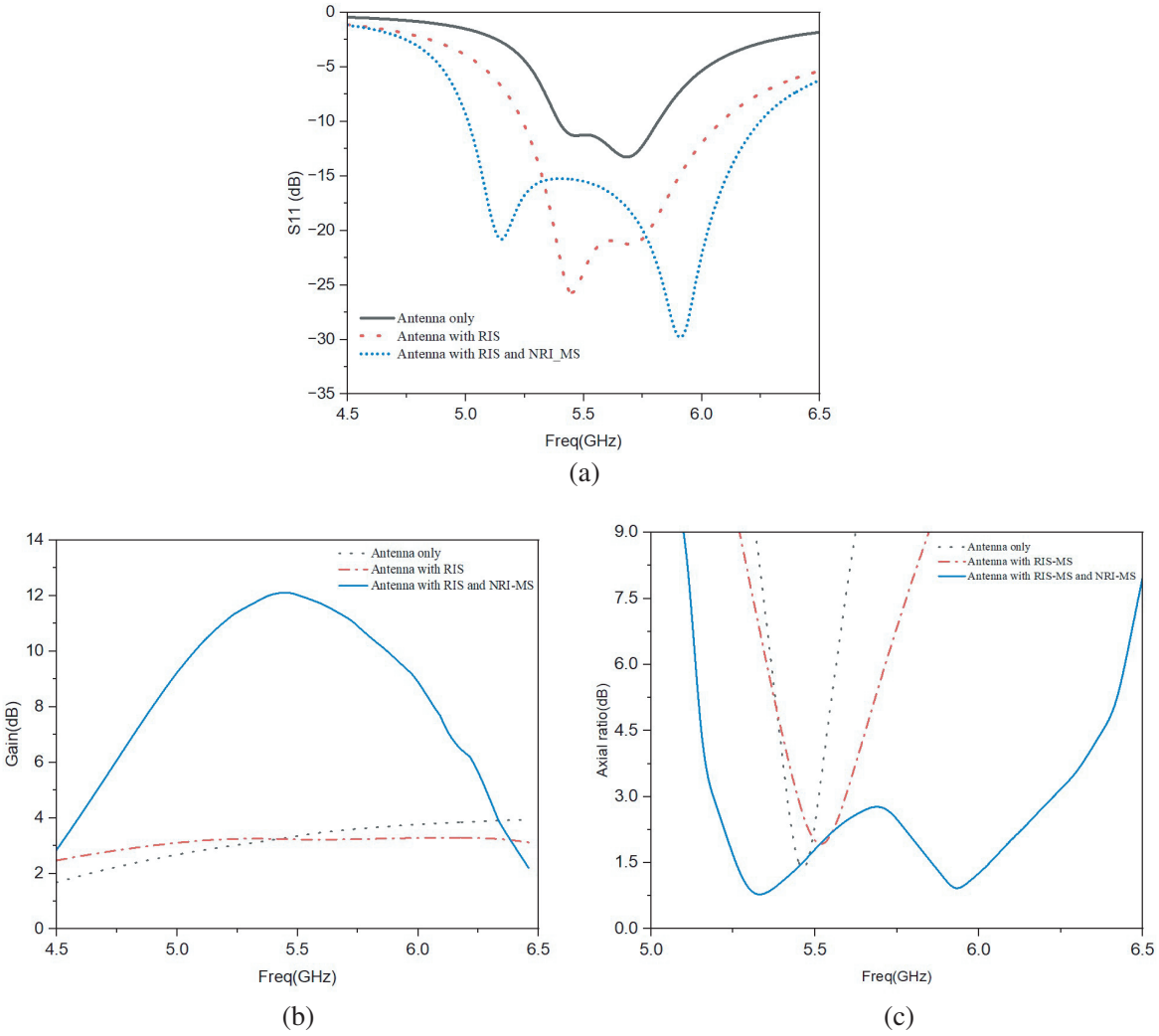

Figure 9. The simulated results of antenna only, antenna with RIS-MS, antenna with RIS-MS and NRI-MS (a) S_{11}, (b) gain, (c) axial ratio bandwidth (ARBW).

Table 1. Comparison of simulation results of proposed antennas.

S. No	Antenna	IBW (%)	Gain (dBic)	ARBW (%)
1	Antenna only	7.84% (5.39 GHz–5.83 GHz)	3	1.09% (5.47 GHz–5.53 GHz)
2	Antenna with RIS-MS	14.66% (5.24 GHz–6.24 GHz)	4	2.72% (5.44 GHz–5.59 GHz)
3	Antenna with RIS-MS and NRI-MS	21.8% (5.01 GHz–6.23 GHz)	12.14	17.09% (5.19 GHz–6.16 GHz)

from 5.19 to 6.16 GHz. Table 1 presents a comparative analysis of the performance outcomes achieved by the proposed antenna versus conventional antennas.

The parameter denoted as resonant distance (h) typically refers to the distance between the

radiating source and the superstrate, as defined in [15].

$$h = \frac{\varphi_1 + \varphi_2}{\pi}\frac{\lambda}{4} + N\frac{\lambda}{2}, \quad N = 0, 1, 2, 3, \ldots \tag{6}$$

The reflection phase of the ground plane is denoted as φ_1, the reflection phase of the metamaterial denoted as φ_2, and the operating wavelength denoted as λ. Given that the ground plane of the radiating source is composed of a metallic conductor, it can be inferred that the reflection phase of the source (patch) is approximately equal to π. Consequently, Equation (6) may be simplified to its reduced form.

$$h = \left(1 + \frac{\varphi}{\pi}\right)\frac{\lambda}{4} \tag{7}$$

At a resonating frequency of 5.5 GHz, the working wavelength is determined to be 54.5 mm. Additionally, the reflection phase of the radiating patch may be adjusted within the range of 0 to π. Therefore, the maximum distance separating the source and the superstrate is equal to half the wavelength ($\lambda/2$). In this work, we see that the highest achievable gain is 12.14 dBic when the separation between the radiating patch and the superstrate layer is approximately equal to half the wavelength, $\lambda/2$. An observable enhancement in gain and variation in reflection coefficient was noted when the distance between the SLPA and NRI-MS increased from 20 mm to 50 mm. In the resonant frequency range, it has been reported that a resonance distance of 30.2 mm results in an impedance bandwidth of 21.8% (5.01–6.23 GHz) and a peak gain of 12.14 dBic.

4. FABRICATION AND RESULTS

An FR4 substrate is used in the fabrication process of the SLPA antenna, as well as the RIS-MS and NRI-MS components of the antenna design. Teflon rods are used for mechanical support, and this configuration creates a cavity between the radiator and NRI-MS. The fabricated prototype of proposed antenna is shown in Figure 10. The presence of Teflon rods does not have any influence on radiation properties of the antenna. In the frequency band ranging from 4.5 GHz to 6.5 GHz, a vector network analyzer is used for the purpose of measuring the reflection coefficient (S_{11}) of the antenna under consideration. The proposed antenna's gain is calculated using the gain transfer technique.

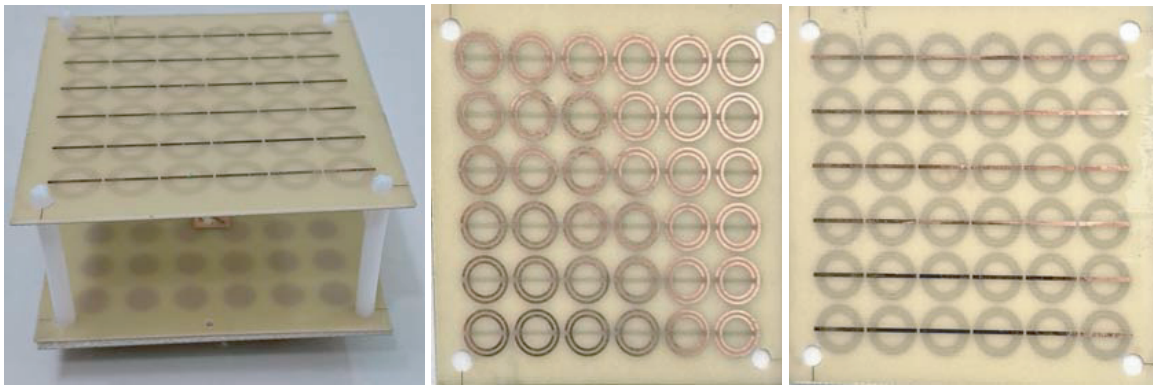

(a) (b) (c)

Figure 10. (a) Fabricated prototype of proposed antenna. (b) Top view of NRI-MS. (c) Bottom view of NRI-MS.

The results of the simulation and measurement are compared in terms of IBW, 3-dB ARBW, and gain. Figure 11 depicts the magnitudes of the measured and simulated gains, 3-dB ARBWs, and S_{11} (reflection coefficient). It is observed that the simulated IBW ranges from 5.01 GHz to 6.23 GHz. Based on Figure 11(a), the measured impedance bandwidth is between 5.12 and 6.37 GHz, or 21.7%. The maximum gain measured is 13.5 dBic, as shown in Figure 11(b). Figure 11(c) displays measured 3-dB ARBW ranges between 5.19 GHz and 6.23 GHz. The results indicate that the simulated and measured

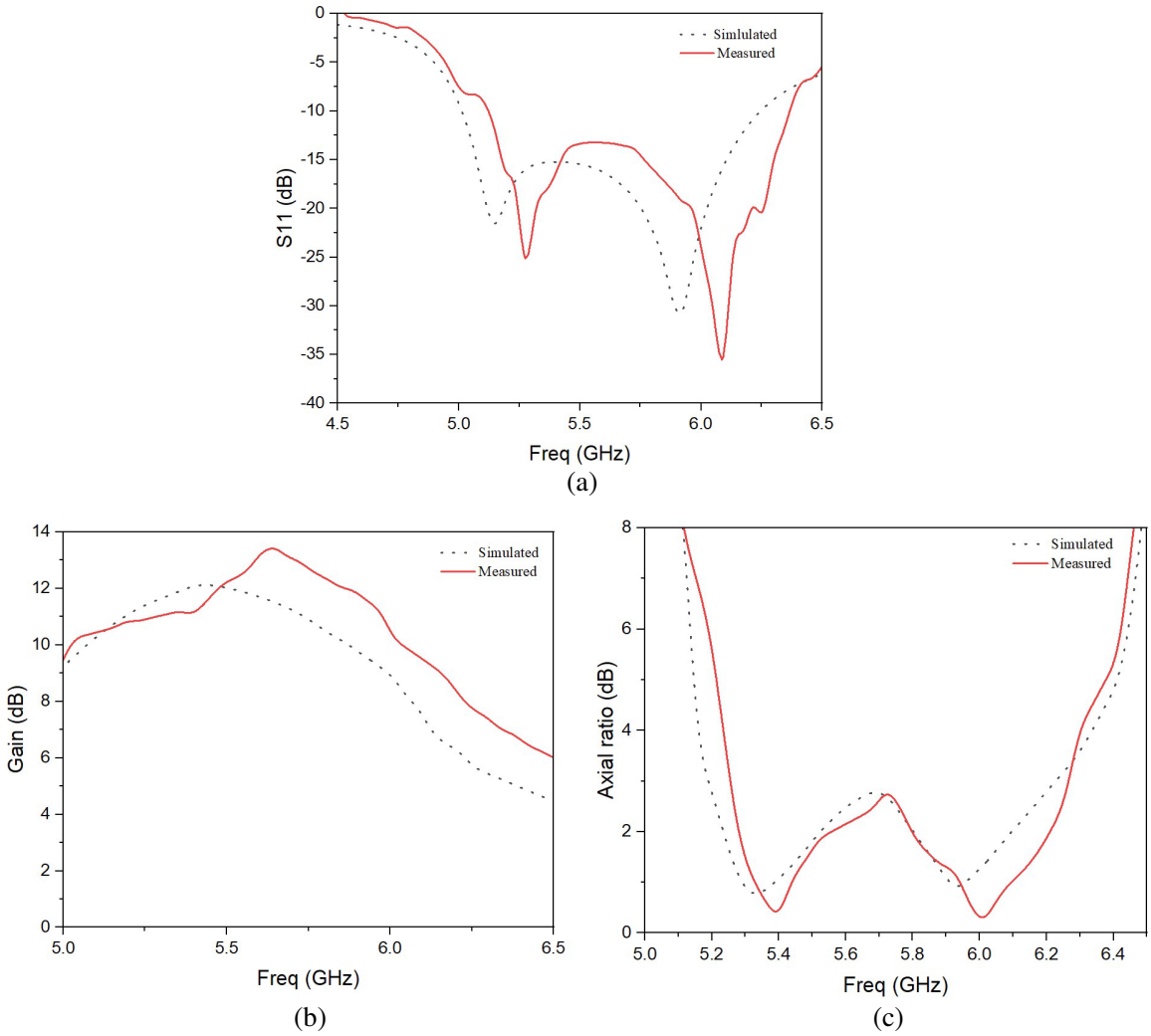

Figure 11. The proposed metasurface antenna simulated and measured results. (a) Reflection coefficient (S_{11}), (b) gain, (c) axial ratio.

Table 2. Comparison of proposed metasurface based CP antenna performance with published literature.

S. No	Ref.	Frequency range (GHz)	Substrate Height (mm)	Gain (dB)	IBW (%)	ARBW (%)	size
1	[5]	9.85–10.1	$\approx \lambda_0/2$	15	2.3%	0.6%	$2.758\lambda_0 * 2.758\lambda_0$
2	[10]	9.24–11.25	$\approx \lambda_0/2$	7.57	7.66%	-	$0.9\lambda_0 * 0.9\lambda_0$
3	[11]	7.04–7.68	$\approx \lambda_0/2$	12.51	6.57%	6.87%	$2.09\lambda_0 * 2.09\lambda_0$
4	[12]	13.1–15.2	$\approx \lambda_0/2$	13	15.5%	-	$3\lambda_0 * 3\lambda_0$
5	[13]	5.01–5.96	$\approx \lambda_0/2$	11.73	17.32%	8.5%	$1\lambda_0 * 1\lambda_0$
6	[16]	5.2–5.8	$\approx \lambda_0/2$	14.2	11.7%	11%	$3\lambda_0 * 3\lambda_0$
7	[17]	8.6–11.2	$\approx \lambda_0/2$	13.8	25%	28%	$2.4\lambda_0 * 2.4\lambda_0$
8	[18]	13.8–15.6	$\approx \lambda_0/2$	20	12%	15%	$4\lambda_0 * 4\lambda_0$
9	[19]	8.2–11	Greater than $\lambda_0/2$	12.5	5%	-	$2.88\lambda_0 * 2.88\lambda_0$
10	Proposed work	5.12–6.37	$\approx \lambda_0/2$	13.5	21.7%	18.2%	$1\lambda_0 * 1\lambda_0$

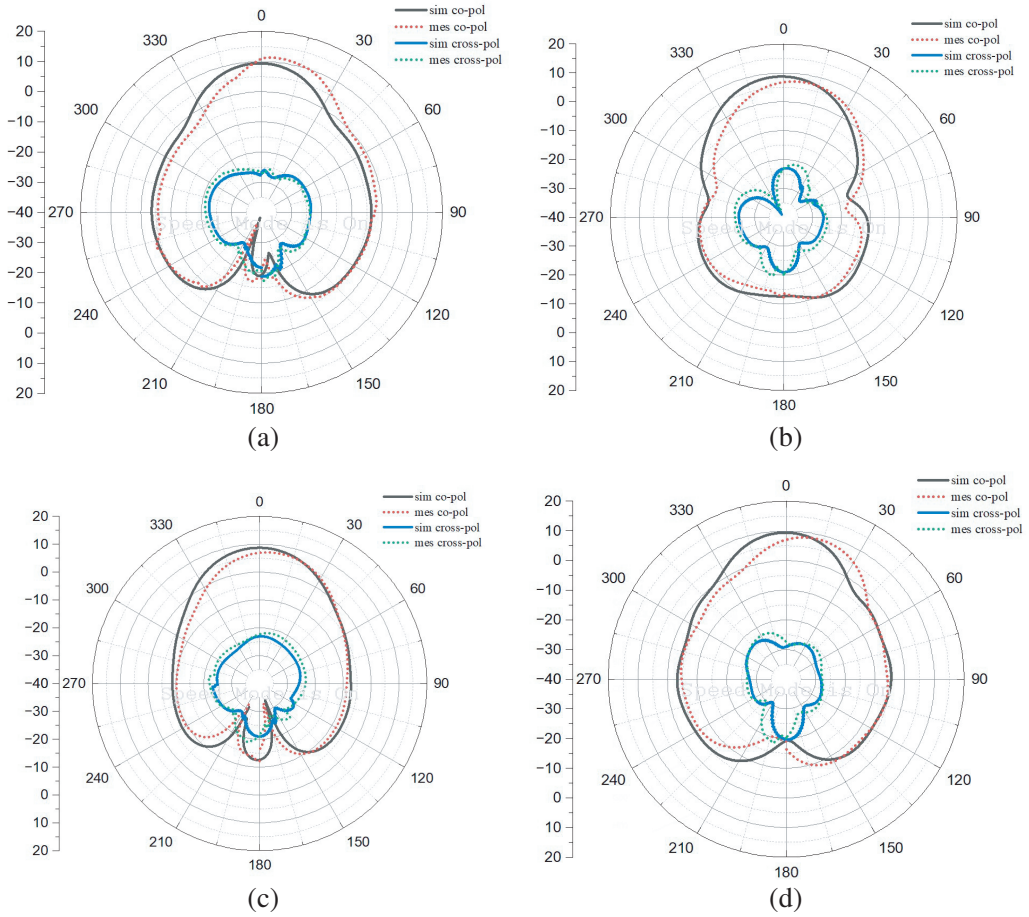

Figure 12. The radiation patterns of the proposed antenna (simulated and measured) at 5.25 GHz, (a) $\phi = 0°$, (b) $\phi = 90°$ and at 5.9 GHz, (c) $\phi = 0°$, (d) $\phi = 90°$.

values are in excellent accordance, with only minor deviations due to connector losses and measurement errors. Figure 12 depicts the antenna's radiation patterns in the E and H planes.

Table 2 provides a comparative analysis between the antenna presented in this paper and existing superstrate based antennas. The proposed antenna uses only an FR-4 epoxy glass substrate, which has low cost and is readily available. It is observed that the proposed RIS-MS and NRI-MS loaded antenna provides more enhanced IBW, ARBW, and gain with less design complexity than existing antennas. The utilization of the NRI-MS superstrate above the antenna and the RIS-MS structure as a ground plane to the antenna results in the simultaneous enhancement of both the gain and bandwidth. The proposed antenna covers the entire 5 GHz frequency band (5.15–5.85 GHz) and is therefore suitable for Wi-Fi and Wi-Max applications in this band.

5. CONCLUSION

In this paper, a circularly polarized SLPA with wide band and high gain is designed and analyzed. RIS-MS and NRI-MS are utilized to simultaneously increase bandwidth and gain. The electromagnetic properties of RIS-MS and NRI-MS unit cells are investigated. Bandwidth is increased by inserting a circular RIS-MS between the patch and ground plane. By placing NRI-MS above the patch, a high gain is obtained, and 3-dB ARBW is also increased. The proposed antenna has an IBW of 21.7% (5.12–6.37 GHz), a 3-dB ARBW of 18.2% (5.19–6.23 GHz), and a peak gain of 13.5 dBic. To verify the simulation results, the proposed antenna is manufactured and tested. A study of the performance of existing antennas and the proposed antennas shows that using metamaterials in antenna design has

the ability to improve antenna parameters. It is evident from the measured results that the proposed RIS-MS and NRI-MS antenna is suitable for 5 GHz WI-FI applications.

ACKNOWLEDGMENT

The authors would like to thank Director, DLRL, DRDO, Hyderabad.

REFERENCES

1. Holloway, C. L., A. M. Dienstfrey, E. F. Kuester, J. F. O'Hara, A. K. Azad, and A. J. Taylor, "A discussion on the interpretation and characterization of metafilms/metasurfaces: The two-dimensional equivalent of metamaterials," *Metamaterials*, Vol. 3, 100–112, 2009.
2. Sievenpiper, D., L. Zhang, R. F. J. Broas, N. G. Alexopolous, and E. Yablonovitch, "High-impedance electromagnetic surfaces with a forbidden frequency band," *IEEE Transactions on Microwave Theory and Techniques*, Vol. 47, No. 11, 2059–2074, 1999.
3. Yang, F.-R., K.-P. Ma, Y. Qian, and T. Itoh, "A uniplanar compact photonic-bandgap (UC-PBG) structure and its applications for microwave circuit," *IEEE Transactions on Microwave Theory and Techniques*, Vol. 47, No. 8, 1509–1514, 1999.
4. Mosallaei, H. and K. Sarabandi, "Antenna miniaturization and bandwidth enhancement using a reactive impedance substrate," *IEEE Transactions on Antennas and Propagation*, Vol. 52, No. 9, 2403–2414, 2004.
5. Nakamura, T. and T. Fukusako, "Broadband design of circularly polarized microstrip patch antenna using artificial ground structure with rectangular unit cells," *IEEE Transactions on Antennas and Propagation*, Vol. 59, No. 6, 2103–2110, 2011.
6. Sarabandi, K., A. M. Buerkle, and H. Mosallaei, "Compact wideband UHF patch antenna on a reactive impedance substrate," *IEEE Antennas and Wireless Propagation Letters*, Vol. 5, 503–506, 2006.
7. Yang, F. and Y. Rahmat-Samii, "A low profile single dipole antenna radiating circularly polarized waves," *IEEE Transactions on Antennas and Propagation*, Vol. 53, No. 9, 3083–3086, 2005.
8. Agarwal, K., N. Nasimuddin, and A. Alphones, "Compact asymmetric slotted-slit patch based circularly-polarized antenna with reactive impedance surface substrate," *Microwave and Optical Technology Letters*, Vol. 54, No. 11, 2505–2510, 2012.
9. Dey, S., S. Mondal, and P. Sarkar, "Reactive impedance surface (RIS) based asymmetric slit patch antenna loaded with complementary split ring resonator (CSRR) for circular polarization," *Journal of Electromagnetic Waves and Applications*, Vol. 33, No. 8, 1003–1013, Feb. 2019.
10. Samantaray, D. and S. Bhattacharyya, "A gain-enhanced slotted patch antenna using metasurface as superstrate configuration," *IEEE Transactions on Antennas and Propagation*, Vol. 68, No. 9, 6548–6556, 2020.
11. Rajanna, P. K. T., K. Rudramuni, and K. Kandasamy, "A high-gain circularly polarized antenna using zero-index metamaterial," *IEEE Antennas and Wireless Propagation Letters*, Vol. 18, No. 6, 1129–1133, 2019.
12. Meriche, M. A., H. Attia, A. Messai, S. S. I. Mitu, and T. A. Denidni, "Directive wideband cavity antenna with single-layer meta-superstrate," *IEEE Antennas and Wireless Propagation Letters*, Vol. 18, No. 9, 1771–1774, 2019.
13. Budarapu, S. K., M. S. Sunder, and B. Ramakrishna, "Performance enhancement of patch antenna using RIS and metamaterial superstrate for wireless applications," *Progress In Electromagnetics Research C*, Vol. 130, 95–105, 2023.
14. Numan, A. B. and M. S. Sharawi, "Extraction of material parameters for metamaterials using a full-wave simulator," *IEEE Antennas and Propagation Magazine*, Vol. 55, No. 5, 202–211, 2013.
15. Trentini, G. V., "Partially reflecting sheet arrays," *IRE Transactions on Antennas and Propagation*, Vol. 4, No. 4, 666–671, 1956.

16. Abdelghani, M. L., H. Attia, and T. A. Denidni, "Dual- and wideband fabry-perot resonator antenna for wlan applications," *IEEE Antennas and Wireless Propagation Letters*, Vol. 16, 473–476, 2017.
17. Wang, N., Q. Liu, C. Wu, L. Talbi, Q. Zeng, and J. Xu, "Wideband fabry-perot resonator antenna with two complementary fss layers," *IEEE Transactions on Antennas and Propagation*, Vol. 62, No. 5, 2463–2471, 2014.
18. Konstantinidis, K., A. P. Feresidis, and P. S. Hall, "Multilayer partially reflective surfaces for broadband Fabry-Perot cavity antennas," *IEEE Transactions on Antennas and Propagation*, Vol. 62, No. 7, 3474–3481, 2014.
19. Singh, A. K., M. P. Abegaonkar, and S. K. Koul, "High-gain and high-aperture efficiency cavity resonator antenna using metamaterial superstrate," *IEEE Antennas and Wireless Propagation Letters*, Vol. 16, 2388–2391, 2017.